



Turbulence of capillary waves — theory and numerical simulation

A.N. Pushkarev^{a,b,*}, V.E. Zakharov^{a,b}

^a Department of Mathematics, University of Arizona, Tucson, AZ 85721, USA

^b L.D. Landau Institute for Theoretical Physics, Russian Academy of Sciences, V-334, ul. Kosygina 2, GSP-1 Moscow 117940, Russia

Received 20 November 1996; received in revised form 1 March 1999; accepted 23 March 1999

Communicated by A.C. Newell

Abstract

An ensemble of weakly interacting capillary waves on a free surface of deep ideal fluid is described statistically by methods of weak turbulence. The stationary kinetic equations for capillary waves have an exact Kolmogorov solution which gives for the spatial spectrum of elevations asymptotics $I_k = C(P^{1/2}/\sigma^{3/4})k^{-19/4}$. The Kolmogorov constant C is found analytically together with the interval of locality in \vec{K} -space. Direct numerical simulation of the dynamical equations in the approximation of small surface angles confirms the presence of almost isotropic Kolmogorov spectrum in the large k region. Besides, at small amplitudes of the pumping, an essentially new phenomenon is found: “frozen” turbulence, in which, despite the big number of interacting waves (of the order of 100) there is no energy flux toward high k . This phenomenon is connected with the finiteness of the region (or, in other words, discreteness of the spectrum in Fourier space). This is believed to be universal for different sorts of nonlinear systems. ©2000 Elsevier Science B.V. All rights reserved.

Keywords: Surface waves; Weak turbulence; Kolmogorov spectra; Kinetic equation for waves

1. Introduction

In this article we study analytically and numerically statistical behavior of an ensemble of capillary waves on a free surface of deep ideal fluid. We have several reasons for this choice of the problem. First of all, capillary waves are a very interesting object by itself. They are the dominating part of surface waves in the conditions of zero gravity. On water surface at the normal gravity, capillary waves are realized in the range of wavelengths

$$0.5 \text{ mm} < \lambda < 17 \text{ mm}. \quad (1)$$

In spite of the relative narrowness of this range, capillary waves play an important role in the dynamics of the sea surface. Only the presence of surface tension prevents wavebreaking at arbitrary small wind [1]. Capillary waves are pumped by gravity waves and carry the energy flux to small scales [2,3]. Generation of capillary waves was observed experimentally [4].

Apart from this discussion, the role of capillary waves on the surface of superfluid helium has to be discussed. Surface tension coefficient for liquid helium is smaller than for water in order of magnitude [5]. However, due

* Corresponding author.

to absence of the viscosity (superfluidity), the minimal wavelength is compatible to atomic size and the range of capillary wave vectors reaches five decades.

On the other hand, studying capillary waves is an interesting problem from the view point of general nonlinear wave dynamics. Capillary waves are a classical example of strongly dispersive waves with powerlike “decay” type of the dispersion law propagating in an isotropic medium. According to the weak-turbulent theory (see, for instance [6]), statistical property of an ensemble of weakly interacting capillary waves can be described by the kinetic equation for squared wave normal amplitudes $n_{\vec{k}}$:

$$\frac{\partial n_{\vec{k}}}{\partial t} + \gamma_{\vec{k}} n_{\vec{k}} = st(n_{\vec{k}}, n_{\vec{k}}). \quad (2)$$

Here $\gamma_{\vec{k}}$ is a damping (or pumping) for waves, $st(n_{\vec{k}}, n_{\vec{k}})$ is the “collision term”, describing pure resonant three-wave interactions.

The stationary damping-free kinetic equation

$$st(n_{\vec{k}}, n_{\vec{k}}) = 0$$

has a powerlike isotropic Kolmogorov solution

$$n_{\vec{k}} = C \frac{P^{1/2}}{\sigma^{1/4}} k^{-17/4}. \quad (3)$$

Here P is the energy flux to the large \vec{K} region, σ the surface tension coefficient, and C the “Kolmogorov constant” to be found analytically.

For the elevation correlation function

$$I_k = \langle |\eta_k|^2 \rangle = \frac{1}{2k^{1/2}\sigma^{1/2}} (n_k + n_{-k}) \quad (4)$$

in the symmetric case, one gets

$$I_k = C \frac{P^{1/2}}{\sigma^{3/4}} k^{-19/4}. \quad (5)$$

It is assumed in Eqs. (2)–(5) that the density of fluid is $\rho = 1$.

The spectrum (3), (5) was found by Zakharov and Filonenko in 1967 [7]. The analytical theory of weak-turbulent Kolmogorov spectra is far advanced now (see [6]). At the same time experimental and numerical evidences, supporting this theory, are rather poor. The only experimental confirmation of weak-turbulent spectra is Toda’s energy dependence on frequency, in the experimentally measured energy spectrum, for gravity waves on the surface of deep water [8],

$$E_\omega \simeq \frac{f(\theta)}{\omega^4}, \quad (6)$$

where $f(\theta)$ is a function of the angle. The Kolmogorov spectrum for a direct cascade of energy is

$$E_\omega \simeq \frac{1}{\omega^4} \quad (7)$$

as found analytically by Zakharov and Filonenko [9]. This coincidence cannot be considered as a complete experimental confirmation of the theoretical result (7) because the Toba spectrum (6) is essentially anisotropic.

Thus, the theory of weak turbulence essentially needs further experimental confirmations. The following questions should be answered:

1. Are the statistical properties of a weakly nonlinear wave field described by the kinetic equation?

2. How good are idealized isotropic Kolmogorov spectrum fits, for the description of the real anisotropic picture of wave turbulence?
3. How important is the influence of the discreteness of the wave spectrum, stemming from the finite size of the physical domain where turbulence is studied?

These questions can be formulated for any possible kind of weak turbulence including turbulence of capillary waves. An alternative approach for answering these question, beside physical experiments, is direct numerical simulation of *dynamical* equations describing a wave system.

In this article we present results of such numerical experiments which have taken several hundreded hours on a CRAY-90 together with a revised theory of the Komogorov spectrum (3)–(5). We will show that this Kolmogorov spectrum is indeed realized in the region of large wavenumbers and is applicable to essentially anisotropic situations, as well as isotropic situations. Moreover, we perform analytic computation of the Kolmogorov constant C and define an “interval of locality”. This allows us to estimate corrections to the Kolmogorov spectrum due to finiteness of the inertial interval.

Numerical simulation of surface waves must include solutions of the boundary problem for the Laplace equation at every time-step. Even in two-dimensional geometry, it is an extremely time-consuming procedure, which becomes unrealistic in the three-dimensional case. We can essentially shorten time of computation using *approximate* dynamical equations, obtained by expansion of the Hamiltonian in powers of nonlinearity (characteristic angle to the horizontal plane), up to second order terms. It is most economical to perform this expansion in canonical variables which are the shape of the surface and the hydrodynamical potential on the surface. Even in such formulations the problem is rather time-consuming. Moreover, the mathematical models of free surface obtained by expansion of the Hamiltonian in powers of nonlinearity, are very unstable numerically. This fact was established by many authors (see [11–13]).

To overcome the numerical instability we introduce “low-pass filtration” equivalent to including artificial damping in the system. As a result, we are able to reach only a moderate level of nonlinearity (characteristic angle of the surface $\theta \simeq 2 \times 10^{-2}$) and to widen the inertial interval only to the scale of a half-decade ($k_{\max}/k_{\min} \simeq 3$). In spite of these strict conditions we positively observed the Kolmogorov spectrum (3) in the inertial interval $8 < k < 23$.

The Kolmogorov spectrum is robust with respect to anisotropy of pumping. If the level of nonlinearity is high enough, it is even robust with respect to discreteness of the wave system as well. Thus, we can be sure that weak-turbulent Kolmogorov spectra are actually adequate for description of wide classes of physical situations, in situations where the kinetic equation (2) actually applies.

The last point is far from trivial. In all our calculations the Kolmogorov spectrum coexists with the spectrum of another, “frozen” type, concentrated in the region of low wavenumbers and fastly decreasing to large wavenumbers. If the level of nonlinearity is low enough, such “frozen” regimes are dominant. In our opinion such spectra are sustained due to nonresonant wave interaction–generation of high-order intensively absorbing beatings. If the pumping is an external force (instead of instability), nonresonant spectra are just Kolmogorov–Arnold–Moser (KAM) tori. Thus, in the case when wave domain is restricted, applicability of the pure kinetic equation (2) is questionable and has to be specially justified. We explain “frozen” regimes of turbulence with the help of maps of quasi-resonances.

A brief description of the results of this article was published in [10].

2. Dynamical equations

The potential flow of an ideal incompressible fluid with free surface is described by the Laplace equation

$$\Delta\phi = 0 \tag{8}$$

with boundary conditions on the surface and bottom of the fluid

$$\frac{\partial \eta}{\partial t} + \nabla_{\perp} \phi \nabla_{\perp} \eta = \frac{\partial \phi}{\partial z} \Big|_{z=\eta}, \quad (9)$$

$$\frac{\partial \phi}{\partial t} + \frac{1}{2} (\nabla \phi)^2 \Big|_{z=\eta} + g\eta - \sigma \operatorname{div} \frac{\nabla_{\perp} \eta}{\sqrt{1 + (\nabla_{\perp} \eta)^2}} = 0, \quad (10)$$

$$\frac{\partial \phi}{\partial z} \Big|_{z \rightarrow -\infty} \rightarrow 0, \quad (11)$$

where $\eta = \eta(\vec{r}, t)$, $\phi = \phi(\vec{r}, t)$ are the shape of the surface and velocity potential, $\vec{r} = (x, y)$, $\vec{v} = \nabla \phi$ and $\nabla_{\perp} = (\partial/\partial x, \partial/\partial y)$; g and σ are the gravity acceleration and surface tension.

The solution of the three-dimensional Cauchy problem (8)–(11) is possible, in principle by numerical integration of the Laplace equation at each time step. This becomes an extremely time-consuming computational problem, especially for simulation of long-time evolution of surface waves turbulence.

It is possible, however, to reduce this problem to a two-dimensional system of two dynamical pseudo-differential equations, using some simplifying assumptions motivated by actual observations of the ocean surface. That simplification tremendously eases the computational aspects of the problem, while keeping all major nonlinear effects.

We introduce the velocity potential, evaluated on the free surface: $\psi(\vec{r}, t) = \phi(\eta(\vec{r}, t), \vec{r}, t)$. Then in terms of the functions η , ψ , the fluid is a Hamiltonian system:

$$\frac{\partial \eta}{\partial t} = \frac{\delta H}{\delta \psi}, \quad (12)$$

$$\frac{\partial \psi}{\partial t} = -\frac{\delta H}{\delta \eta}, \quad (13)$$

where H is total energy of the fluid consisting of the kinetic and the potential components

$$H = H_{\text{pot}} + H_{\text{kin}}, \quad H_{\text{pot}} = \frac{1}{2} g \int \eta^2 d\vec{r} + \sigma \int \left(\sqrt{1 + (\nabla \eta)^2} - 1 \right) d\vec{r}, \quad H_{\text{kin}} = \frac{1}{2} \int d\vec{r}_{\perp} \int_{-\infty}^{\eta} dz (\nabla \phi)^2. \quad (14)$$

Now we make the above mentioned simplifying assumption: steepness of the surface is small, i.e. $|\nabla \eta| \ll 1$. It is important to mention that many measurements of the ocean surface steepness give the mean square value of the characteristic angle of the surface as $\langle \theta^2 \rangle \simeq 10^{-2} - 10^{-3}$.

Under this assumption the Hamiltonian can be expanded, using small parameter $|\nabla \eta|$:

$$H = H_0 + H_1 + H_2 + \dots,$$

$$H_0 = \frac{1}{2} \int \left[|k| |\psi_{\vec{k}}|^2 + (g + \sigma |k|^2) |\eta_{\vec{k}}|^2 \right] d\vec{k},$$

$$H_1 = -\frac{1}{2} \frac{1}{2\pi} \int L_{\vec{k}_1 \vec{k}_2} \psi_{\vec{k}_1} \psi_{\vec{k}_2} \eta_{\vec{k}_3} \delta(\vec{k}_1 + \vec{k}_2 + \vec{k}_3) d\vec{k}_1 d\vec{k}_2 d\vec{k}_3,$$

$$H_2 = -\frac{1}{4(2\pi)^2} \int M_{\vec{k}_1 \vec{k}_2 \vec{k}_3} \psi_{\vec{k}_1} \psi_{\vec{k}_2} \eta_{\vec{k}_3} \delta(\vec{k}_1 + \vec{k}_2 + \vec{k}_3) d\vec{k}_1 d\vec{k}_2 d\vec{k}_3,$$

$$L_{\vec{k}_1 \vec{k}_2} = \vec{k}_1 \vec{k}_2 + |\vec{k}_1| |\vec{k}_2|,$$

$$M_{\vec{k}_1 \vec{k}_2 \vec{k}_3 \vec{k}_4} = |\vec{k}_1| |\vec{k}_2| \left[\frac{1}{2} \left[|\vec{k}_1 + \vec{k}_3| + |\vec{k}_1 + \vec{k}_4| + |\vec{k}_2 + \vec{k}_3| + |\vec{k}_2 + \vec{k}_4| \right] - |\vec{k}_1| - |\vec{k}_2| \right],$$

where we have used the following normalization of Fourier transforms and the δ -function:

$$\psi_k = \frac{1}{\sqrt{2\pi}} \int \psi_x e^{-ikx} dx,$$

$$\psi_x = \frac{1}{\sqrt{2\pi}} \int \psi_k e^{ikx} dk,$$

$$\delta(x) = \frac{1}{2\pi} \int e^{ikx} dk.$$

Dynamic equations are

$$\begin{aligned} \frac{\partial \eta_{\vec{r}}}{\partial t} = & [|\hat{k}| \psi]_{\vec{r}} - \operatorname{div}(\eta \nabla \psi) - |\hat{k}| [|\hat{k}| \psi]_{\vec{r}} \times \eta_{\vec{r}}]_{\vec{r}} \\ & + |\hat{k}| [|\hat{k}| [|\hat{k}| \psi]_{\vec{r}} \times \eta_{\vec{r}}]_{\vec{r}} \times \eta_{\vec{r}}]_{\vec{r}} + \frac{1}{2} \Delta_{\vec{r}} [|\hat{k}| \psi]_{\vec{r}} \times \eta_{\vec{r}}^2]_{\vec{r}} + \frac{1}{2} |\hat{k}| [\Delta_{\vec{r}} \psi \times \eta_{\vec{r}}^2], \end{aligned} \quad (15)$$

$$\begin{aligned} \frac{\partial \psi_{\vec{r}}}{\partial t} = & -g \eta_{\vec{r}} + \sigma \operatorname{div} \frac{\nabla \eta}{\sqrt{1 + (\nabla \eta)^2}} + \frac{1}{2} [-(\nabla \psi)^2 + [|\hat{k}| \psi]_{\vec{r}}^2] - |\hat{k}| [|\hat{k}| \psi]_{\vec{r}} \times \eta_{\vec{r}}]_{\vec{r}} \times [|\hat{k}| \psi]_{\vec{r}} \\ & - \Delta \psi \times [|\hat{k}| \psi]_{\vec{r}} \times \eta_{\vec{r}} \end{aligned} \quad (16)$$

corresponding to Hamiltonian

$$\begin{aligned} H = & \frac{1}{2} \int [|\hat{k}| \psi]_{\vec{r}} \times \psi_{\vec{r}} + g \eta_{\vec{r}}^2 + 2\sigma \left(\sqrt{1 + (\nabla \eta_{\vec{r}})^2} - 1 \right) - \left([|\hat{k}| \psi]_{\vec{r}}^2 - (\nabla \psi_{\vec{r}})^2 \right) \times \eta_{\vec{r}} \\ & + [|\hat{k}| \psi]_{\vec{r}} \times \eta_{\vec{r}} \times \left(|\hat{k}| [|\hat{k}| \psi]_{\vec{r}} \times \eta_{\vec{r}} \right) + \Delta \psi [|\hat{k}| \psi]_{\vec{r}} \times \eta_{\vec{r}}^2] d\vec{r}. \end{aligned}$$

Brackets $[\dots]_{\vec{r}}$ denote an expression in R -space. The action of the operator $|\hat{k}|$ on the function $\psi_{\vec{r}}$ is defined by

$$[|\hat{k}| \psi]_{\vec{r}} = \frac{1}{2\pi} \int |k| \psi_{\vec{k}} e^{i\vec{k}\vec{r}} d\vec{k}.$$

3. Weak-turbulent approach

Introduction of normal canonical variables

$$\eta_{\vec{k}} = \sqrt{\frac{\omega_k}{2(g + \sigma k^2)}} (a_{\vec{k}} + a_{-\vec{k}}^*), \quad \psi_{\vec{k}} = -i \sqrt{\frac{g + \sigma k^2}{2\omega_k}} (a_{\vec{k}} - a_{-\vec{k}}^*)$$

diagonalizes the Hamiltonian H_0 and reduces the system of equations (15) and (16) to one complex equation

$$\frac{\partial a_k}{\partial t} + i \frac{\delta H}{\delta a_k^*} = 0. \quad (17)$$

For the capillary-dominating limit $k \gg \sqrt{g/\sigma}$, Eq. (17), in linear approximation, describes capillary waves with the dispersion relation

$$\omega_k = \sqrt{\sigma} k^\alpha, \quad \alpha = \frac{3}{2}$$

which is of “decaying” type, which means that one can simultaneously satisfy the relations

$$\omega_{\vec{k}} = \omega_{\vec{k}_1} + \omega_{\vec{k}_2}, \quad (18)$$

$$\vec{k} = \vec{k}_1 + \vec{k}_2 \quad (19)$$

for any possible choice of vectors \vec{k} , \vec{k}_1 , \vec{k}_2 . At this point the theory starts to deviate significantly for capillary and gravitational waves cases (in the gravity case the system (18) and (19) has no solutions).

In capillary case, the first nonlinear correction H_1 is the dominating one in the weakly nonlinear situation and one can use a statistical description for the stochastic wave field, or a weak-turbulent theory. According to the weak-turbulent theory the correlation function

$$\langle a_{\vec{k}} a_{\vec{k}'} \rangle = n_k \delta(\vec{k} - \vec{k}')$$

satisfies the kinetic equation for waves (2) which takes, in capillary waves case, the form [7]

$$\frac{\partial n_{\vec{k}}}{\partial t} = st(n_{\vec{k}}), \quad (20)$$

$$st(n_{\vec{k}}) = \int \left[R_{\vec{k}\vec{k}_1\vec{k}_2} - R_{\vec{k}_1\vec{k}\vec{k}_2} - R_{\vec{k}_2\vec{k}\vec{k}_1} \right] d\vec{k}_1 d\vec{k}_2, \quad (21)$$

$$R_{\vec{k}\vec{k}_1\vec{k}_2} = 4\pi |V_{\vec{k}\vec{k}_1\vec{k}_2}|^2 \delta(\vec{k} - \vec{k}_1 - \vec{k}_2) \delta(\omega_{\vec{k}} - \omega_{\vec{k}_1} - \omega_{\vec{k}_2}) \left[n_{\vec{k}_1} n_{\vec{k}_2} - n_{\vec{k}} n_{\vec{k}_1} - n_{\vec{k}} n_{\vec{k}_2} \right], \quad (22)$$

$$V_{\vec{k}\vec{k}_1\vec{k}_2} = \frac{1}{8\pi\sqrt{2\sigma}} (\omega_k \omega_{k_1} \omega_{k_2})^{1/2} \left[\frac{L_{\vec{k}_1, \vec{k}_2}}{(k_1 k_2)^{1/2} k} - \frac{L_{\vec{k}, -\vec{k}_1}}{(k k_1)^{1/2} k_2} - \frac{L_{\vec{k}, -\vec{k}_2}}{(k k_2)^{1/2} k_1} \right], \quad (23)$$

$$L_{\vec{k}_1, \vec{k}_2} = \vec{k}_1 \vec{k}_2 + k_1 k_2. \quad (24)$$

We are looking for the solutions of kinetic equation (20) symmetrical with respect to rotations in wave vector space \vec{k} [6]. To get these solutions, we should average the kinetic equation over the angles of wave vectors in \vec{K} -space. This averaging consists in calculation of the integrals of products of $|V|^2$ and the δ -function over the angles in \vec{K} -space and can be trivially done due to the fact that matrix element (23) depends only on products of functions of absolute values of wave vectors and trigonometric functions of the angles.

Multiplying Eq. (20) by $k(dk/d\omega)$ and averaging over angles in \vec{k} -space one can get, after variables transformation $k(\omega) = \omega^{1/\alpha}/\sigma^{1/2\alpha}$:

$$\frac{\partial \eta_k}{\partial t} = \frac{1}{k(dk/d\omega)} \int \left[S_{\omega\omega_1\omega_2} \delta(\omega - \omega_1 - \omega_2) (n_{\omega_1} n_{\omega_2} - n_{\omega} n_{\omega_2} - n_{\omega} n_{\omega_1}) - S_{\omega_1\omega\omega_2} \delta(\omega_1 - \omega - \omega_2) (n_{\omega} n_{\omega_2} - n_{\omega_1} n_{\omega_2} - n_{\omega} n_{\omega_1}) - S_{\omega_2\omega\omega_1} \delta(\omega_2 - \omega - \omega_1) (n_{\omega} n_{\omega_1} - n_{\omega_1} n_{\omega_2} - n_{\omega} n_{\omega_2}) \right] d\omega_1 d\omega_2, \quad (25)$$

$$S(\omega, \omega_1, \omega_2) = \frac{1}{32\pi\alpha^3\sigma^{3/\alpha+1}} (\omega\omega_1\omega_2)^{2/\alpha} \langle |U_{\vec{k}, \vec{k}_1, \vec{k}_2}|^2 \delta(\vec{k} - \vec{k}_1 - \vec{k}_2) \rangle, \quad (26)$$

where

$$\begin{aligned} \langle |U_{\vec{k}, \vec{k}_1, \vec{k}_2}|^2 \delta(\vec{k} - \vec{k}_1 - \vec{k}_2) \rangle &= \int_0^{2\pi} \int_0^{2\pi} \left[\frac{L_{\vec{k}_1, \vec{k}_2}}{(k_1 k_2)^{1/2} k} - \frac{L_{\vec{k}, -\vec{k}_1}}{(k k_1)^{1/2} k_2} - \frac{L_{\vec{k}, -\vec{k}_2}}{(k k_2)^{1/2} k_1} \right]^2 \delta(\vec{k} - \vec{k}_1 - \vec{k}_2) d\phi_1 d\phi_2 \\ &= \frac{2}{k^2} \frac{\left[\left(1 + \frac{1 - \xi_1^{2/\alpha} - \xi_2^{2/\alpha}}{2\xi_1^{1/\alpha} \xi_2^{1/\alpha}} \right) (\xi_1 \xi_2)^{1/2\alpha} - \left(1 - \frac{1 + \xi_1^{2/\alpha} - \xi_2^{2/\alpha}}{2\xi_1^{1/\alpha} \xi_2^{1/\alpha}} \right) \xi_1^{1/2\alpha} - \left(1 - \frac{1 + \xi_2^{2/\alpha} - \xi_1^{2/\alpha}}{2\xi_2^{1/\alpha} \xi_1^{1/\alpha}} \right) \xi_2^{1/2\alpha} \right]^2}{\sqrt{4\xi_1^{2/\alpha} \xi_2^{2/\alpha} - \left(1 - \xi_1^{2/\alpha} - \xi_2^{2/\alpha} \right)^2}}, \end{aligned} \quad (27)$$

where ϕ_1 and ϕ_2 are the angles of vectors \vec{k}_1, \vec{k}_2 in \vec{K} -space, $S(\omega, \omega_1, \omega_2)$ is a homogeneous function of the power $\gamma = \frac{8}{3}$:

$$S(\epsilon\omega, \epsilon\omega_1, \epsilon\omega_2) = \epsilon^\gamma S(\omega, \omega_1, \omega_2). \quad (28)$$

Suppose that the stationary solution of Eq. (20) has the form of a power function

$$n_\omega = A\omega^x. \quad (29)$$

To determine this form, one can make a conformal transformation in the second term of the right-hand side of Eq. (25)

$$\omega_1 = \frac{\omega^2}{\omega'_1}, \quad \omega_2 = \frac{\omega\omega'_2}{\omega'_1} \quad (30)$$

and in the third term

$$\omega_1 = \frac{\omega\omega'_1}{\omega'_2}, \quad \omega_2 = \frac{\omega^2}{\omega'_2}. \quad (31)$$

Taking into account that Jacobians of the transformation equations (30) and (31) are $|(\omega/\omega'_1)^3|$ and $|(\omega/\omega'_1)^3|$, the collision integral (21) can be reduced to

$$\begin{aligned} st[n] = & \frac{A^2}{k(dk/d\omega)} \int S_{\omega_1, \omega_2, \omega_3} \delta(\omega - \omega_1 - \omega_2) [(\omega_1\omega_2)^x - (\omega\omega_1)^x - (\omega\omega_2)^x] \\ & \times \left[1 - \left(\frac{\omega}{\omega_1}\right)^y - \left(\frac{\omega}{\omega_2}\right)^y \right] d\omega_1 d\omega_2, \end{aligned}$$

where $y = \gamma + 2x + 2$. In dimensionless form, this can be written as

$$st[n] = \frac{A^2}{16\pi\alpha^2\sigma^{1/\alpha+1}} \omega^{y-2/\alpha} I(y), \quad (32)$$

$$\begin{aligned} I(y) = & \int (\xi_1\xi_2)^{2/\alpha} [1 - \xi_1^{-y} - \xi_2^{-y}] [(\xi_1\xi_2)^x - \xi_1^x - \xi_2^x] \delta(1 - \xi_1 - \xi_2) \\ & \times \frac{\left[\left(1 + \frac{1 - \xi_1^{2/\alpha} - \xi_2^{2/\alpha}}{2\xi_1^{1/\alpha}\xi_2^{1/\alpha}} \right) (\xi_1\xi_2)^{1/2\alpha} - \left(1 - \frac{1 + \xi_1^{2/\alpha} - \xi_2^{2/\alpha}}{2\xi_1^{1/\alpha}\xi_2^{1/\alpha}} \right) \frac{\xi_1^{1/2\alpha}}{\xi_2^{1/\alpha}} - \left(1 - \frac{1 + \xi_2^{2/\alpha} - \xi_1^{2/\alpha}}{2\xi_2^{1/\alpha}\xi_1^{1/\alpha}} \right) \frac{\xi_2^{1/2\alpha}}{\xi_1^{1/\alpha}} \right]^2}{\sqrt{4\xi_1^{2/\alpha}\xi_2^{2/\alpha} - \left(1 - \xi_1^{2/\alpha} - \xi_2^{2/\alpha} \right)^2}} d\xi_1 d\xi_2. \end{aligned} \quad (33)$$

The collision integral is finite or interaction is local (i.e., only scales close to each other contribute to the integral) when the integral $I(y)$ is finite. This integral converges for $-5 < x < \frac{5}{6}$ and becomes zero at $x = -1$ and $x = -\frac{17}{4}$ (see Fig. 1). Both solutions are obvious — one appears as a requirement of the first bracket in the integrand to be zero ($y = -1$). The second appears from the requirement of the second bracket to be zero ($x = -1$).

Solution $x_0 = -1$ is the thermodynamically equilibrium Rayleigh–Jeans distribution corresponding to the fluxless regime of turbulence and is not physically important. Solution $y = -1$, or $x_1 = -\frac{17}{6}$ corresponds to the finite energy flux from the pumping region at large scales to the damping region at small scales.

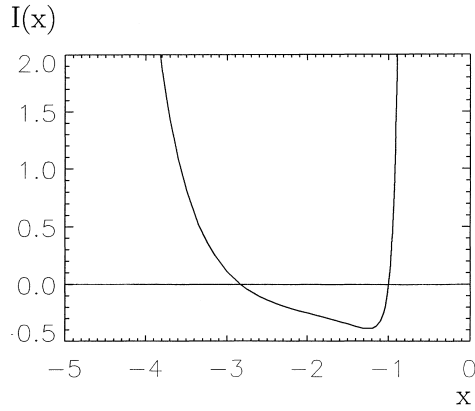


Fig. 1. Collision integral I as a function of power solution index x : it is finite within the locality interval $-5 < x < -5/6$ and has two zeros at $x_0 = -1$ (thermodynamical spectrum) and $x = -\frac{17}{4}$ (Kolmogorov solution).

One should note that index x_0 of thermodynamical solution lies inside the locality interval and the Kolmogorov solution index x_1 is located not exactly at the center of the locality interval.¹

The continuity equation for the spectral energy density $\epsilon_\omega = \omega N_\omega$ is

$$\frac{\partial \epsilon_\omega}{\partial t} + \frac{\partial P}{\partial \omega} = 0, \tag{34}$$

where N_ω is the spectral density of the number of particles.

Using the integral relation $\int N_\omega d\omega = \int n_{\vec{k}} d\vec{k}$, which becomes in the axial-symmetrical case $N_\omega = n_k 2\pi k (dk/d\omega)$, we get for energy flux P corresponding to power solution (29):

$$P = - \int \omega N_\omega d\omega = - \frac{A^2}{8\alpha^3 \sigma^{2/\alpha+1}} \frac{\omega^{y+1}}{y+1} I(y). \tag{35}$$

The last expression contains, however, the singularity $\frac{0}{0}$ at the point $y = -1$, which can be resolved by the L'Hopital rule:

$$P = - \frac{A^2}{8\alpha^3 \sigma^{2/\alpha+1}} \left. \frac{\partial I}{\partial y} \right|_{y=-1}. \tag{36}$$

From the dimensional estimate

$$n_k = C \frac{\sqrt{P}}{\sigma^{1/4}} k^{-17/4},$$

where C is the dimensionless universal Kolmogorov constant. Comparing this relation with the power spectrum $n_k = A\omega^{x_0} = A\sigma^{x_0/2} k^{\alpha x_0}$, we get the expression for the Kolmogorov constant:

$$C = \frac{2\sqrt{2}\alpha^{3/2}}{\sqrt{-\frac{\partial I}{\partial y}|_{y=-1}}}, \tag{37}$$

¹ In [6] is mentioned that "... Kolmogorov exponent always lies exactly in the middle of the locality interval", which is not always true: it is realized only in the case when thermodynamical index does not belong in the locality interval.

where

$$\frac{\partial I}{\partial y} \Big|_{y=-1} = \int_0^1 d\xi (\xi(1-\xi))^{2/\alpha} [\xi \log \xi + (1-\xi) \log(1-\xi)] \times \left[(\xi(1-\xi))^{-17/6} - \xi^{-17/6} - (1-\xi)^{-17/6} \right] \\ \times \frac{\left[\left(1 + \frac{1-\xi^{2/\alpha} - (1-\xi)^{2/\alpha}}{2\xi^{1/\alpha}(1-\xi)^{1/\alpha}} \right) (\xi(1-\xi))^{1/2\alpha} - \left(1 - \frac{1+\xi^{2/\alpha} - (1-\xi)^{2/\alpha}}{2\xi^{1/\alpha}} \right) \frac{\xi^{1/2\alpha}}{(1-\xi)^{1/\alpha}} - \left(1 - \frac{1+(1-\xi)^{2/\alpha} - \xi^{2/\alpha}}{2(1-\xi)^{1/\alpha}} \right) \frac{(1-\xi)^{1/2\alpha}}{\xi^{1/\alpha}} \right]^2}{\sqrt{4\xi^{2/\alpha}(1-\xi)^{2/\alpha} - (1-\xi^{2/\alpha} - (1-\xi)^{2/\alpha})^2}}$$

Evaluating the last integral numerically, we get

$$C = 9.85. \quad (38)$$

4. Numerical model

Our model of gravity–capillary waves is based on the system of equations (15) and (16) supplied with damping (viscous) term $D_{\vec{r}}$ and forcing term $F_{\vec{r}}$:

$$\frac{\partial \eta_{\vec{r}}}{\partial t} = [|\hat{k}|\psi]_{\vec{r}} - \operatorname{div}(\eta \nabla \psi) - |\hat{k}|[|\hat{k}|\psi]_{\vec{r}} \times \eta_{\vec{r}} + |\hat{k}|[|\hat{k}|[|\hat{k}|\psi]_{\vec{r}} \times \eta_{\vec{r}}]_{\vec{r}} \times \eta_{\vec{r}} + \frac{1}{2} \Delta_{\vec{r}} [|\hat{k}|\psi]_{\vec{r}} \times \eta_{\vec{r}}^2 \\ + \frac{1}{2} |\hat{k}| [\Delta_{\vec{r}} \psi \times \eta_{\vec{r}}^2], \quad (39)$$

$$\frac{\partial \psi_{\vec{r}}}{\partial t} = -g\eta_{\vec{r}} + \sigma \operatorname{div} \frac{\nabla \eta}{\sqrt{1 + (\nabla \eta)^2}} + \frac{1}{2} [-(\nabla \psi)^2 + [|\hat{k}|\psi]_{\vec{r}}^2] - |\hat{k}|[|\hat{k}|\psi]_{\vec{r}} \times \eta_{\vec{r}} + [|\hat{k}|\psi]_{\vec{r}} - \Delta \psi \\ \times [|\hat{k}|\psi]_{\vec{r}} \times \eta_{\vec{r}} + D_{\vec{r}} + F_{\vec{r}}. \quad (40)$$

The Fourier-component of $F_{\vec{r}}$ was chosen in two different forms,

$$F_{1\vec{k}} = f_{\vec{k}} \cos((1 + R(t))\omega_k t) \quad (41)$$

and

$$F_{2\vec{k}} = \Gamma(\vec{k})\psi_{\vec{k}}, \quad \Gamma(\vec{k}) > 0, \quad (42)$$

where $\omega_k = \sqrt{(g + \sigma k^2)\vec{k}}$ is the local linear frequency, $R(t)$ is a function of time, taking values randomly distributed between -1 and $+1$; $\Gamma(\vec{k}) > 0$ is the growth rate of forcing.

The Fourier-component of physical damping, or viscous term is defined by

$$D_{\vec{k}} = \gamma_k \psi_k, \quad \gamma_k < 0 \quad (43)$$

and is not important for our purposes for the reasons explained below.

Eqs. (39) and (40) constitute a Hilbert-differential system of equations, which was solved numerically in operator form, using pseudo-spectral technique based on fast Fourier transform (FFT) algorithm. This choice of spatial solution of the system was defined by preference of FFT, as an economical algorithm for calculation of integrals of convolution type. The idea of this algorithm can be illustrated on the example of calculation of the term $[|\hat{k}|\psi]_{\vec{r}}$:

1. Calculate $\psi(\vec{k}) = \operatorname{FFT}(\psi(\vec{r}))$.
2. Multiply $\psi(\vec{k})$ by $|\hat{k}|$ in \vec{K} -space.
3. Calculate $[|\hat{k}|\psi]_{\vec{r}} = \operatorname{FFT}^{-1}[|\hat{k}| \times \psi(\vec{k})]$.

4. Calculate $[|k|\psi]_{\vec{r}}^2$: Using this approach one can calculate all necessary nonlinear terms in the right-hand side of Eqs. (39) and (40) from known functions $\psi(\vec{r})$ and $\eta(\vec{r})$ at each time-step.

The most unpleasant surprise of numerical simulation of surface waves consists in the fact that a wide variety of numerical schemes approximating the system (39) and (40) easily become nonlinearly numerically unstable. In other words, short-wave perturbations to long-wave flow start to grow if the long-wave flow is strong enough. In particular, among the numerical schemes we tried, is the one-parameter family of implicit numerical schemes exactly preserving the Hamiltonian.

Observed numerical instability is not new: the same type of instability, we believe, was observed in previous publications [11–13]. This instability can be, however, suppressed up to certain amplitudes of background flow, using low-pass filtering of the function $\eta_{\vec{k}}, \psi_{\vec{k}}$, which suppresses the high-wavenumbers part of the spectrum while keeping the small-wavenumbers part of the spectrum unchanged. In other words, at each time-step, these functions are multiplied by

$$R_k = e^{-(k/k_0)^n}, \quad n = 10, \quad k_0 = 0.7\text{--}0.9 k_{\max},$$

where k_{\max} is the maximum wavenumber in the problem.

This filtering is equivalent to introducing extra damping terms $\epsilon_k \eta_{\vec{k}}$ and $\epsilon_k \psi_{\vec{k}}$ in the right-hand side of Eqs. (39) and (40) respectively, where

$$\epsilon_k = \frac{1 - R_k^{-1}}{\tau}. \quad (44)$$

It is possible to show that this damping is much stronger than the physical damping. As confirmed by numerical experiments, this is responsible for the major part of energy absorption in the system. Therefore we resist using the physical viscous term (43) in equations. Another way of diminishing the instability effect is decreasing the time-step of integration.

To advance in time, the predictor–corrector numerical scheme of the second order was used as a computationally low-cost alternative to implicit schemes. Calculations were carried out on the grid 256×256 in the region of \vec{R} -space $2\pi \times 2\pi$ with periodical boundary conditions.

5. “Frozen” turbulence regime

A series of experiments were carried out with the pumping (41) localized at small wavenumbers. These showed that at low levels of nonlinearity, $(H_1 + H_2)/H_0 \leq 10^{-3}$, there is a stationary regime of “frozen” turbulence in the small-wavenumbers region of pumping with exponentially decaying spectrum toward high \vec{k} . The wave spectrum consists of several dozens of excited low-wavenumber harmonics, possibly exchanging energy between each other, without generating energy cascade toward high-wavenumbers. There is virtually no energy absorption associated with high-wavenumbers damping in that case.

We interpret this regime as generic, associated with wave spectrum discreteness due to the periodicity of boundary conditions and explain it in Section 7. The characteristic feature of this regime is formation of ring structures around $\vec{k} = 0$ (see Fig. 2).

We think that such frozen regimes of turbulence can be realized in nature in bounded systems like lakes and finite-size laboratory resonators and could be detected experimentally by testing for the presence of ring structures in the spectrum of surface elevations.

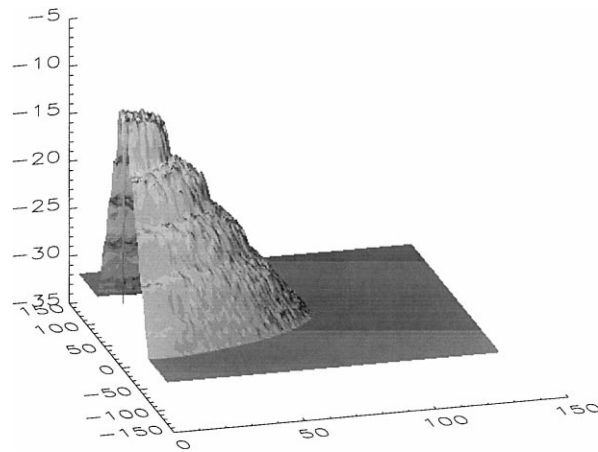


Fig. 2. One half of the spectrum of spatial elevation in the case of frozen turbulence.

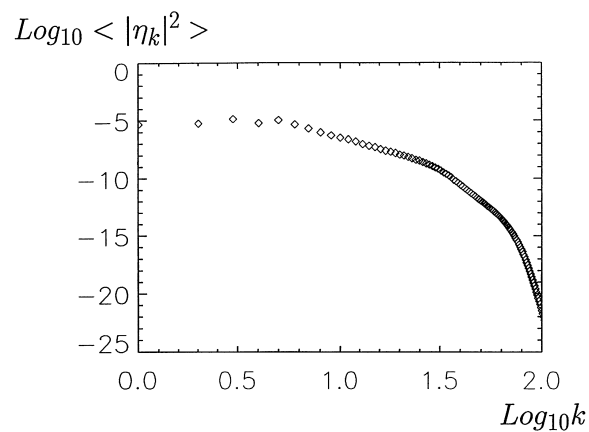


Fig. 3. Logarithm of the spectrum of spatial elevations of the liquid surface as a function of the logarithm of wavenumber.

It is tempting to identify the frozen turbulence with the KAM regime in Hamiltonian systems of many degrees of freedom. This comparison can be done only with caution because in our case the system is not conservative and is pumped in a random way.

6. Kolmogorov turbulence

A different regime of turbulence occurs at higher levels of nonlinearity $(H_1 + H_2)/H_0 \simeq 10^{-2}$. The stationary spectrum is angular isotropic in this case and transfers a finite energy flux to the large- \vec{k} region (see Fig. 3).

The plot of the logarithmic derivative (see Fig. 4) shows that in the interval $8 < k < 23$ the spectrum can be considered as powerlike $I_k = qk^{-x}$. The exponential value is close to $x \simeq 4.8$, $q \simeq 0.03$.

From weak-turbulent theory $q = C_{\text{exp}}\sqrt{P}$ ($\sigma = 1$), where C_{exp} is an experimental value of the Kolmogorov constant. Once we have measured the energy flux P , we can calculate C_{exp} and compare its value with Eq. (38).

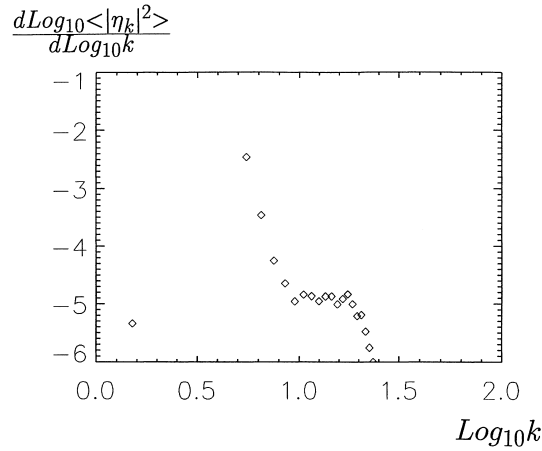


Fig. 4. The derivative of the logarithm of the spectrum of spatial elevations with respect to logarithm of the wavenumber as a function of the logarithm of the wavenumber (the local value of the Kolmogorov index).

Energy absorption, or flux is given by

$$P = \frac{\partial E}{\partial t} \int \frac{1 - R_k^{-1}}{\tau} \left(|k| |\psi_k|^2 + \sigma k^2 |\eta_{\vec{k}}|^2 \right) d\vec{k}, \quad (45)$$

where τ is the time-step of the numerical scheme and R_k is a low-pass filter. The flux P measured according to these formulae is $P \simeq 3 \times 10^{-4}$ which gives the experimental value of the Kolmogorov constant

$$C_{\text{exp}} = 1.7.$$

The strong deviation between the experimental value of the Kolmogorov constant from its theoretical value can be explained by the narrowness of the inertial interval realized in numerical simulation: a significant part of waves born in the small-wavenumber region of the pumping is absorbed directly at the large-wavenumber region.

Let us consider this point in more detail. Eqs. (15) and (16) describe, in particular, four-wave nonresonant process in which three waves with wavenumbers $\vec{k}_1, \vec{k}_2, \vec{k}_3$ generate nonresonant beating, with wavenumber

$$\vec{k}_b = \vec{k}_2 + \vec{k}_3 - \vec{k}_1.$$

If all \vec{k}_i ($i = 1, 2, 3$) are inside the ring $|k_i| \leq k_a$, the maximum value of k_b is $k_b \simeq 3k_a$. In the case when k_b is placed in the zone of strong damping, dissipation in $k \simeq k_b$ can provide an intensive flux of energy away from the domain $k \simeq k_a$.

A detailed theory of this process (including five- and six-wave interactions) will be published in a separate article. We just mention that these nonresonant processes of direct skipping of energy to large \vec{k} are vanishing at $k_{\text{max}} \rightarrow \infty$. However, in our experiments, the flux of energy measured by formula (45) is overestimated, with respect to the energy flux responsible for the Kolmogorov spectrum. Such deviation between experimental and theoretical values for the Kolmogorov constant should also asymptotically disappear at $k_{\text{max}} \rightarrow \infty$.

The experiments were also carried out for the “growth rate” pumping (42) in the isotropical case

$$\Gamma_{\vec{k}} = A e^{-((k-k_0)/k_0)^4}$$

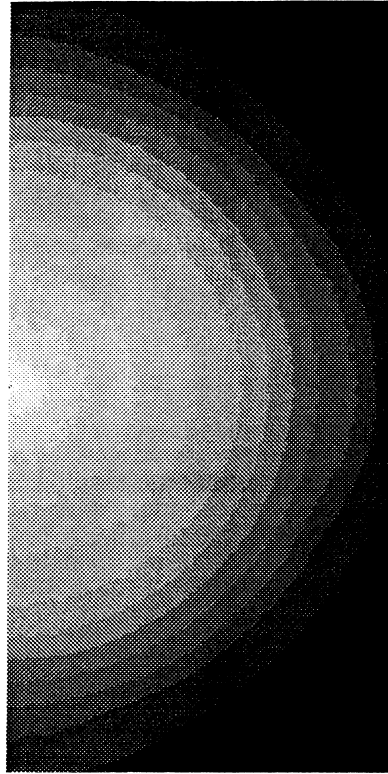


Fig. 5. Density plot of one half of two-dimensional spectrum of spatial elevations in the case of anisotropic growth rate pumping.

and anisotropic case

$$\Gamma_{\vec{k}} = \begin{cases} Ae^{-((k-k_0)/k_0)^4}, & \text{if } -\frac{\pi}{4} < \phi < \frac{\pi}{4}, \\ 0, & \text{otherwise,} \end{cases}$$

where A is real amplitude and ϕ is polar angle in the plane (k_x, k_y) .

In both cases the stationary spectrum obeys angular isotropy (see Fig. 5) with the part described by the Kolmogorov law (see Fig. 6).

Finally, one should mention that the observed picture of stationary spectra was invariant with respect to the damping and pumping parameters change in an acceptable range.

7. Maps of quasi-resonances

The above numerical experiments have demonstrated that the theory of weak turbulence is correct in the two-dimensional case, as well as the existence of the Kolmogorov spectrum. This result is confirmed by data of laboratory experiments carried out in the Department of Physics, UCLA [14].

Still, there are several questions to be answered:

1. Difference of the experimental value of the Kolmogorov constant from the theoretical one.
2. Existence of fluxless or frozen turbulence regimes at very low levels of short-wave forcing.

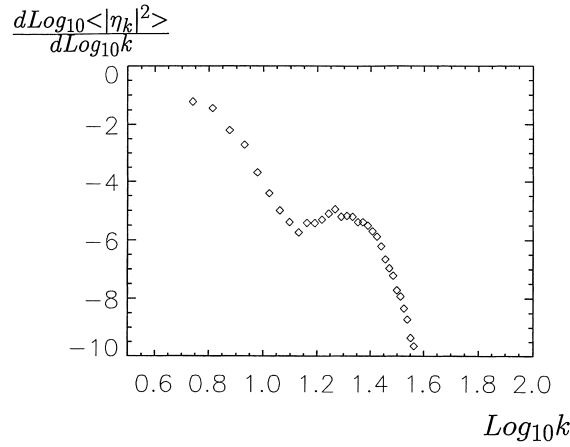


Fig. 6. Same as Fig. 4, but in the case of anisotropic growth rate pumping.

3. “Wedding cake” shape of the frozen turbulence spectrum (Fig. 2) which gives an oscillating one-dimensional spectrum after angle-averaging.

Below we show that a simple kinematic consideration helps to understand the answers to these questions.

An interaction of the Fourier modes in kinetic equation for capillary waves is performed through the interaction of triplets of waves which are solutions of the system of equations (18) and (19), usually referred by “conservation laws” or “resonances”. This system always has solutions in the case of a continuous spectrum for dispersion relation of capillary waves (18), known as “decay-type” dispersion relation [6].

The situation is changed, however, in the case of finite domain. Fourier harmonics of the system with periodical boundary conditions are not continuous functions of the wavenumber anymore, like in the case of infinite domain, but an infinite set of values defined at discrete equidistant wavenumbers. The question of existence of the solution of the system (18) and (19) turns into a, generally speaking, nontrivial number theory problem. A significant breakthrough in classification of existence of solutions of this system for different types of dispersion relations $\omega_{\vec{k}}$ was obtained by Kartashova [15]. It was shown, in particular, that the system (18) and (19) does not have solutions in the case of capillary waves dispersion relation (18), which means that there are no interacting Fourier modes in the kinetic equation for waves in the finite domain.

The situation is changed, however, if nonlinear dispersion correction δ_k due to finite amplitude of the excited wave is taken into account and capillary wave frequency becomes

$$\omega_k = \sigma^{1/2} k^{3/2} + \delta_k. \quad (46)$$

Conservation laws (18) and (19) are transformed into “quasi-conservation laws” or “quasi-resonances”:

$$\omega_{k_1} + \omega_{k_2} - \omega_{k_3} = \Delta_{k_1 k_2 k_3}, \quad (47)$$

$$\vec{k}_1 + \vec{k}_2 = \vec{k}_3, \quad (48)$$

$$\Delta_{k_1 k_2 k_3} = \delta_{k_3} - \delta_{k_1} - \delta_{k_2}. \quad (49)$$

It is clear that the system (47)–(49) has many more degrees of freedom than the system (18) and (19) in the sense of existence of solutions due to variability of parameter $\Delta_{k_1 k_2 k_3}$ which is the effective level of excitation of oscillations.

To understand the answers to the above questions, we propose two modifications of the algorithm of searching of solutions of the system (47)–(49). Each algorithm builds the two-dimensional “map” in Fourier space which marks solutions of this system by “0” and “1”.

The first type of two-dimensional map function represents all possible triplets:

$$\vec{k}_1 = (k_{1x}, k_{1y}), \quad (50)$$

$$\vec{k}_2 = (k_{2x}, k_{2y}), \quad (51)$$

$$\vec{k}_3 = (k_{3x}, k_{3y}), \quad (52)$$

given fixed vector \vec{k}_3 . Under this assumption quasi-resonances (47)–(49) transform into

$$(k_{1x}^2 + k_{1y}^2)^{3/4} + \left((k_{3x} - k_{1x})^2 + (k_{3y} - k_{1y})^2 \right)^{3/4} - (k_{3x}^2 + k_{3y}^2)^{3/4} = \Delta.$$

Map function $M_1^\epsilon(k_x, k_y)$ is defined by

$$M_1^\epsilon(\vec{k}_1) = \begin{cases} 1, & \text{if } |\Delta| \leq \epsilon, \\ 0, & \text{if } |\Delta| > \epsilon. \end{cases}$$

Every map $M_1^\epsilon(k_x, k_y)$ corresponds to a chosen “level” of the turbulence ϵ . The algorithm of building of the map is nothing but testing if triplet $\vec{k}_1, \vec{k}_2, \vec{k}_3$ has discrepancy Δ less than ϵ . If the answer is “yes” all points $\vec{k}_1, \vec{k}_2, \vec{k}_3$ are assigned the value of 1, and 0 otherwise.

Fig. 7(a)–(c) represents $M_1^\epsilon(\vec{k})$ for three different values of ϵ . The resonance curve practically disappears with diminishing excitation level ϵ which means that the number of allowed triplets decreases significantly with decrease of the level of excitation of waves.

Another type of map function represents all possible triplets $\vec{k}_1, \vec{k}_2, \vec{k}_3$ on two-dimensional Fourier plane. The corresponding equation for quasi-resonances becomes

$$(k_{1x}^2 + k_{1y}^2)^{3/4} + (k_{2x}^2 + k_{2y}^2)^{3/4} - \left((k_{1x} + k_{2x})^2 + (k_{1y} + k_{2y})^2 \right)^{3/4} = \Delta_{k_1 k_2}$$

and the map function is defined by

$$M_2^\epsilon(\vec{k}_1) = \begin{cases} 1, & \text{if } |\Delta| \leq \epsilon \text{ for some } \vec{k}_2, \\ 0, & \text{if } |\Delta| > \epsilon \text{ for all } \vec{k}_2. \end{cases}$$

Similar to the previous case, map $M_2^\epsilon(\vec{k})$ corresponds to a particular “level” of the turbulence ϵ and is nothing but testing if any triplet’s $\vec{k}_1, \vec{k}_2, \vec{k}_3$ discrepancy Δ is less than ϵ . If it is the case, all points $\vec{k}_1, \vec{k}_2, \vec{k}_3$ are assigned the value of 1, and 0 otherwise.

It is important to note that, generally speaking, a particular map is also a function of cutoff wavenumber in Fourier space k_{cut} which is the characteristic value of the starting of significant high-wavenumber damping. The bigger is k_{cut} , the more resonances exist on the map. This is clear from the following consideration. Suppose that the absolute value of \vec{k}_1 is much smaller than \vec{k}_2, \vec{k}_3 . It is clear that the bigger k_{cut} , the more possibilities exist to satisfy the condition $\Delta < \epsilon$ for any given ϵ .

Fig. 8(a–c) shows the maps of quasi-resonances for $\epsilon = 0.0001, \epsilon = 0.01, \epsilon = 1.0$. White areas correspond to allowed Fourier modes while black ones to prohibited ones. As one could expect, the richness of resonances grow significantly with the growth of ϵ . The picture of resonances in Fig. 8(a) is very poor — direct analysis shows that there are no two different triplets $\vec{k}_1, \vec{k}_2, \vec{k}_3$ coupling with each other. This case corresponds to the case of pure

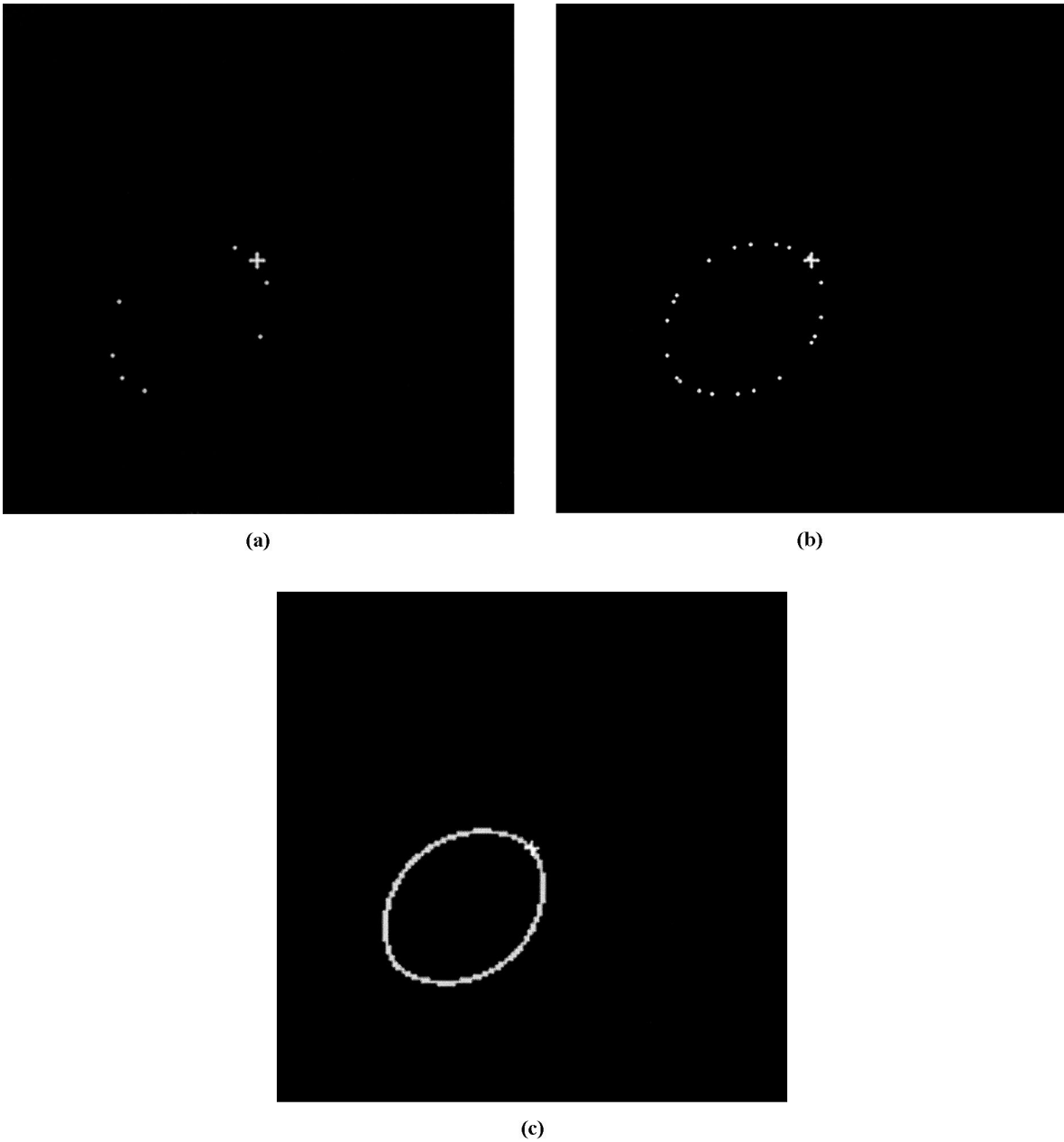


Fig. 7. (a) Map of quasi-resonances $M_1^\epsilon(k_x, k_y)$ for $\epsilon = 0.1$. Point $k_x = 0, k_y = 0$ is located at the center of the picture and marked by a white cross. White areas correspond to 1 (allowed modes), black areas to 0 (prohibited modes); (b) same as (a) but for $\epsilon = 1$; (c) same as (a), but for $\epsilon = 10$.

frozen turbulence, because there is no mechanism of energy transfer from one triplet to another, i.e. from low to high wavenumbers.

The picture of resonances in Fig. 8(b) is significantly denser. It was found that there are coupling triplets of wavevectors in this case able to transfer the energy from low to high wavenumbers, still not many. It is interesting that averaging the map over the angle in Fourier space gives an oscillatory one-dimensional “wave spectrum” due

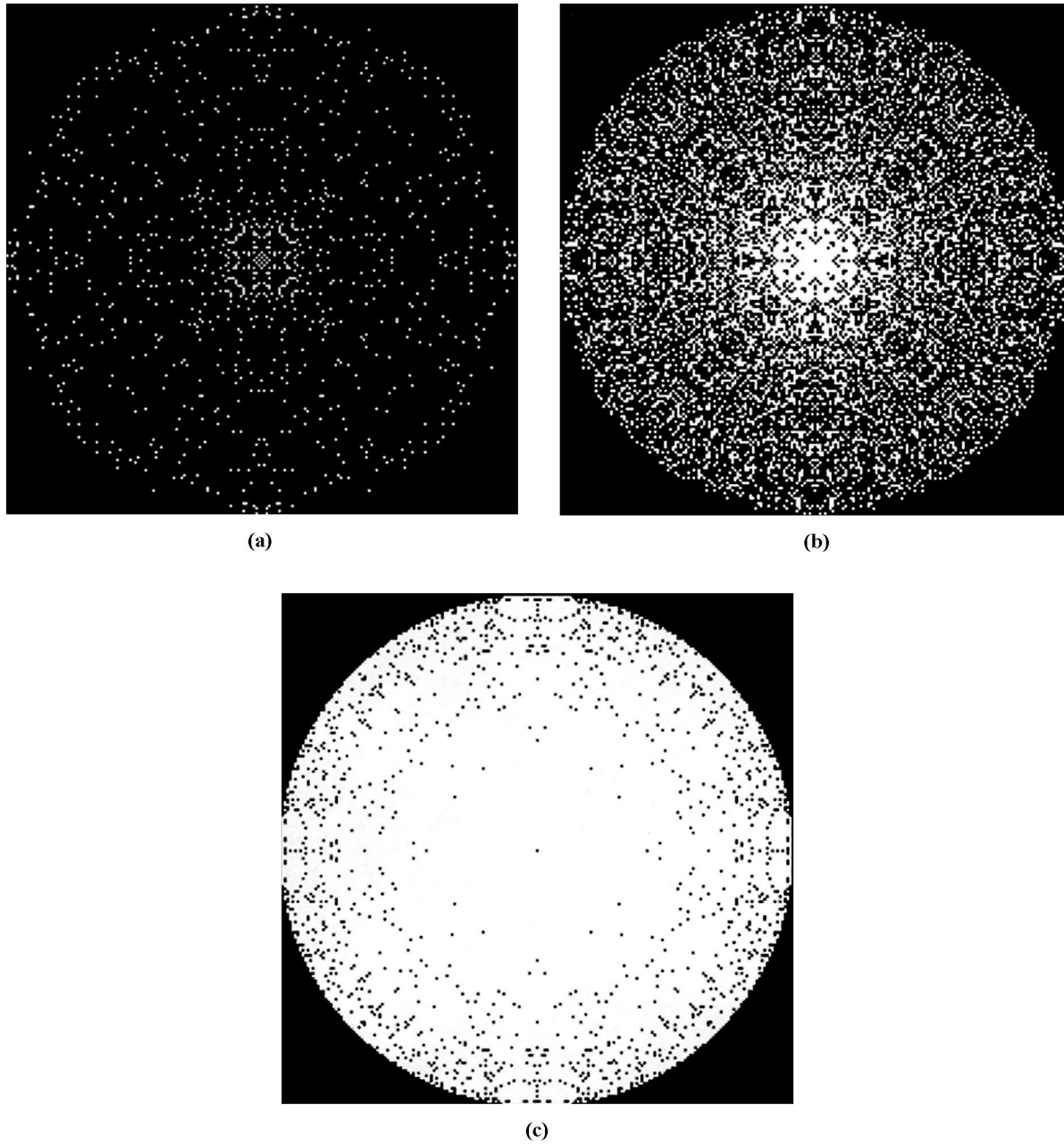


Fig. 8. (a) Map of quasi-resonances $M_2^\epsilon(k_x, k_y)$ for $\epsilon = 0.0001$. Point $k_x = 0, k_y = 0$ is located at the center of the picture. White areas correspond to 1 (allowed modes), black areas to 0 (prohibited modes); (b) same as (a) but for $\epsilon = 0.01$; (c) same as (a), but for $\epsilon = 1.0$.

to the presence of spectral holes on the corresponding two-dimensional map. It is tempting, but difficult to compare these oscillations with low-wavenumber oscillations in laboratory data [14], where some of the low-wavenumber oscillations are produced by effects of parametric forcing. Still, the tendency of formation of oscillatory spectrum is quite obvious in numerical experiments (see Fig. 2) and represents an interesting subject of investigation in laboratory experiments.

The map of resonances in Fig. 8(c) presents the case of well-developed coupling of resonant triplets. The result of its averaging over the angle does not contain any oscillations. One can expect that the effect of frozen turbulence should be minimal in this case being compared to the cases Fig. 8(a) and (b) which creates better conditions for realization of Kolmogorov regime of turbulence.

8. Conclusion

Our work shows that weak-turbulent theory is correct in the two-dimensional case and the Kolmogorov spectrum occurs. Stationary spectra of capillary wave turbulence are locally isotropical ones, in other words, the spectrum structure in high \vec{k} is independent of the details of the pumping.

At small amplitudes of the pumping principally a new phenomenon takes place: frozen turbulence in which despite the big number of interacting waves (of the order of 100) there is no energy flux generation toward high \vec{k} . This phenomenon is connected with the finiteness of the region (or, in other words, discreteness of the spectrum in Fourier space). It is universal for wave turbulence in limited regions for different sorts of nonlinear systems and can be observed in natural and laboratory experiments detecting, in particular, such macroscopic exhibition as ring structures in Fourier space. The degree of equivalence of the frozen turbulence to KAM regime in conservative dynamical systems presents principal interest.

The mechanism of frozen turbulence can be understood through the analysis of solutions of kinematic three-wave quasi-conservation laws. This analysis is performed numerically by building the maps of quasi-resonances which show that for small levels of excited waves, Fourier space is split into the regions of allowed and prohibited modes, or spectral holes. Presence of spectral holes is the cause of oscillatory behavior of angle-averaged spectra of turbulence. For very small levels of excitation, there are no coupling triplets of the wavevectors responsible for energy transfer from low to high wavenumbers. The number of allowed Fourier modes grows significantly with the increase of the level of excitation and inertial range in Fourier space. As a result, one can expect a Kolmogorov regime of turbulence at relatively high levels of excited waves and big enough inertial range in Fourier space. Weak turbulence with intermediate levels of excitation in bounded systems is therefore, as a rule, the mixture of frozen and Kolmogorov turbulence.

The challenge is to build simplified dynamical numerical model of purely frozen turbulence. It can be based on a numerical algorithm which consists of the solution of dynamical equations coupled with a dynamically changing map of allowed modes in time and Fourier space. It is also tempting to detect such frozen turbulence in laboratory experiments on excitation of capillary waves in containers which could be observed via detection of ring structures in two-dimensional spectra of surface elevations.

Acknowledgements

This work was supported by the Office of Naval Research of the USA (grants N00 14-92-J-1343 and N000 14-98-1-0070) and partially by Russian Basic Research Foundation (grant 94-01-00898). We are using this opportunity to acknowledge these foundations.

Thanks are due to Computational Mechanics Publications for their kind permission to reproduce some parts of this paper which first appeared in [16].

References

- [1] V.E. Zakharov, Direct and inverse cascade in wind-driven sea and wave breaking, in: M.L. Banner, R.H.Y. Grimshaw (Eds.), Proceedings of IUTAM Meeting of Wave Breaking, Sydney, 1991, Springer, Berlin, 1992, pp. 69–91.

- [2] A. Newell, V.E. Zakharov, Rough sea foam, *Phys. Rev. Lett* 69 (1992) 1149–1151.
- [3] K. Watson, J. Bride, Excitation of capillary waves by longer waves, *J. Fluid Mech.* 250 (1993) 103–119.
- [4] B. Jahne, K. Riemer, Two-dimensional wavenumber spectra of small scale water surface waves, *J. Geophysical Res.* 95 (1995) 11531–11546.
- [5] R.J. Donnelly (Ed.), *High Reynolds Number Flows using Liquid and Gaseous Helium*, Springer, New York, 1991.
- [6] V.E. Zakharov, G. Falkovich, V.S. Lvov, *Kolmogorov Spectra of Turbulence I*, Springer, Berlin, 1992.
- [7] V.E. Zakharov, N.N. Filonenko, Weak turbulence of capillary waves, *J. Appl. Mech. Tech. Phys.* 4 (1967) 50–515.
- [8] Y. Toba, Local balance in the air-sea boundary processes III. On the spectrum of wind waves, *J. Oceanogr. Soc. Japan* 29 (1973) 209–220.
- [9] V.E. Zakharov, N.N. Filonenko, The energy spectrum for stochastic oscillation of a fluid surface, *Dokl. Akad. Nauk SSSR* 170(6) (1966) 1292–1295.
- [10] A.N. Pushkarev, V.E. Zakharov, Turbulence of capillary waves, *Phys. Rev. Lett* 76 (1996) 3320–3323.
- [11] M.S. Longuet-Higgins, E.D. Cokelet, *Proc. Roy. Soc. London, Ser. A* 350 (1985) 1.
- [12] D.G. Dommermuth, D. Yue, *J. Fluid Mech.* 184 (1987) 267.
- [13] W. Craig, S. Sulem, Numerical simulation of gravity waves, *J. Computat. Phys.* 108 (1993) 73–83.
- [14] W. Wright, R. Budakian, S. Putterman, *Phys. Rev. Lett.* 76 (24) (1996).
- [15] E. Kartashova, Wave resonances in systems with discrete spectra, in: V.E. Zakharov (Ed.), *Nonlinear Waves and Weak Turbulence, Advances in the Mathematical Sciences (formerly Advances in Soviet Mathematics)*, American Mathematical Society, Providence, RI, 1998, pp. 95–129.
- [16] A.N. Pushkarev, V.E. Zakharov, Turbulence of capillary waves—theory and numerical simulation. Nonlinear ocean waves, in: W. Perrie (Ed.), *Advances in fluid mechanics*, ch. 4, vol. 17, Computational Mechanics Publications, Southampton, Boston, MA, 1998, pp. 111–131.